Parameter Estimation of Human Nerve C-Fibers using Matched Filtering and Multiple Hypothesis Tracking : Complete report

Björn Hammarberg (Hansson) Clemens Forster Erik Torebjörk

rev. 2, July 11, 2000

Abstract—**We describe a multiple target tracking (MTT) application in microneurography that estimate conduction velocity changes and recovery constants of human nerve C-fibers. Results using the tracking system on real data are presented.**

Action potentials (APs) were recorded from C-fibers in the peroneal nerve of awake human subjects. The APs were detected by a matched filter constituting a maximum likelihood constant false alarm rate (ML-CFAR) detector.

Using the multiple hypothesis tracking (MHT) method, the detected APs (targets) in each trace (scan) were associated to individual nerve fibers (tracks) by their typical conduction latencies in response to electrical stimulation. The measurements were one-dimensional (range only) and the APs were spaced in time with intersecting trajectories. In general, the AP amplitude of each C-fiber differed for different fibers. Amplitude estimation was therefore incorporated into the tracking algorithm to improve the performance.

The target trajectory was modeled as an exponential decay with three unknowns. These parameters were estimated iteratively by applying the simplex method on the parameters that enter nonlinearly and the least squares method on the parameters that enter linearly.

Keywords—**Detection, matched filtering, target tracking, MHT, multiple hypothesis tracking, parameter estimation, microneurography**

I. Introduction

IMPROVING signal processing in a real world application in an area where traditional tools are inadequate often generates many new challenges. We will here describe such an application, arising from the need to study the stimulus-response characteristics of peripheral unmyelinated (C-) fibers in human skin nerves. Key tools for the solution were to be found in a seemingly unrelated area, namely radar tracking of multiple targets.

The action potentials (APs) of the C-axons are recorded through a thin needle electrode inserted transcutaneously into the nerve [1] [2]. The APs may be detected as extracellular spikes in this recording. Yet, the signal-to-noise ratio (SNR) is rather poor and the amplitude of some APs is of the same order of magnitude as the peaks of the noise [3]. In such situations special methods are required for the detection.

Neuronal activity is evoked by applying sensory stimuli in the skin area innervated by the fiber of interest. APs originating from other fibers, however, are also recorded by the electrode.[1] Their presence obstructs the study of the stimulus-response characteristics considerably as it is virtually impossible to decide which APs originate from the fiber of interest.

To overcome this problem, Hallin and Torebjörk introduced a method that shows the excitation of a C-fiber by utilizing the so-called *marking phenomenon* [4]. The phenomenon stems from the slight decrease of a fiber's conduction velocity after an AP has been conducted. The conduction velocity then slowly returns to its initial value.

The principle of the method is to apply a distinct stimulus repetitively, at a low frequency (0.25 Hz), into the innervation territory of the C-fiber under study. For each impulse, one single AP is evoked and appears in the recording after a certain latency (Fig. 1, at 303 ms). To document the response characteristics of the C-fiber, a physiological test stimulus (e.g. mechanical, temperature, chemical) is applied into the receptive field of the fiber. If such a stimulus generates additional action potentials, the conduction velocity of the affected fiber decreases. In this case, the AP excited by the repetitive stimuli shows a noticeable increase in latency (Fig. 1, trace 13 to 40). This change in latency is used as a *marker* to indicate that the C-unit has responded to the applied physiological stimulus [5]. In addition, the latency increase provides a semi quantitative estimate of the number of APs that were generated by the test stimulus [6].

To enhance the efficiency of these experiments, a computer-supported recording system is used [7]. For the repetitive stimuli, electrical impulses are used because they are both distinct and excite all different kinds of nerve fibers. The impulses are delivered through needle electrodes positioned in the innervation area of the fiber of interest. Often, several fibers are co-activated and recorded simultaneously, but due to slight differences in conduction velocity of the individual C-fibers, the action potentials are spaced in time in the recorded signal (Fig. 1, at 303 ms and 360 ms). Using the marking phenomenon, it is thus possible to individually identify separate C-fibers and to study their characteristic latency responses.

In the human skin nerves, different types of C-fibers exist [8]. Recently, it has become evident that the latency increase, due to a particular number of impulses, and the time course of their recovery differ in different classes of C-fibers [9]. This finding is intriguing because it may promote new insights into differential properties of membranes in different C-fiber classes in humans.

Previously, the analysis of the recorded traces was carried out manually; a task that was very time consuming. Therefore, a

Björn Hammarberg is with the Signals and Systems Group, Uppsala University, and the Department of Clinical Neurophysiology, University Hospital, Uppsala, Sweden. Email: Bjorn.Hammarberg@signal.uu.se; WWW: http://www.signal.uu.se/Staff/bh/bh.html.

Clemens Forster is with the Institute of Physiology and Experimental Pathophysiology, University of Erlangen, Erlangen, Germany.

Erik Torebjörk is with the Department of Clinical Neurophysiology, University Hospital, Uppsala, Sweden.

Parts of this paper have been published at SPIE Conf. AeroSense '98, Signal and Data Processing of Small Targets, 14-16 April 1998 in Orlando, Florida.

[1] These fibers could be either co-excited by the applied stimuli or spontaneously active.

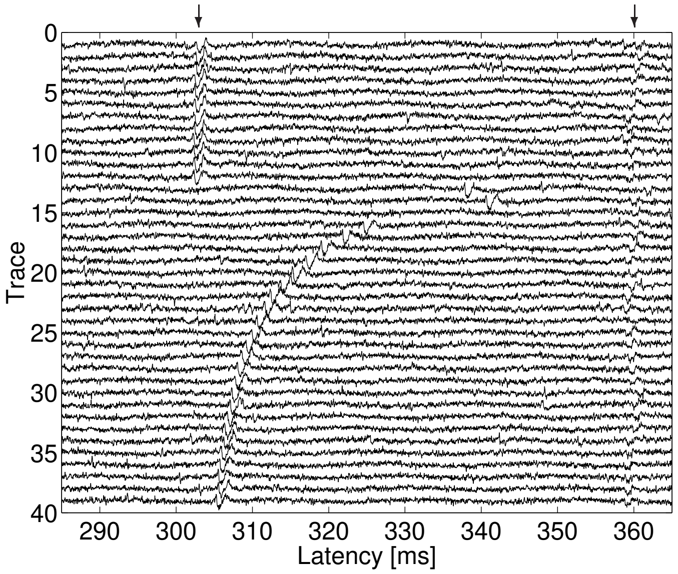

Fig. 1. The APs of two C-fibers with latencies of about 303 ms and 360 ms, respectively, are shown. The responses are excited by electrical stimuli delivered at 0.25 Hz into the skin innervation territory of the fibers. Successive responses are displayed in traces from top to bottom. At trace 13, the left unit is activated in response to a mechanical stimulus leading to a decrease in the conduction velocity, i.e. an increase in latency. Following this, the conduction velocity recovers gradually as indicated by the APs returning to the latency prior to the activation. The right unit does not respond to the applied stimuli and its latency is retained throughout the recording.

computer program that detects the action potentials, discriminates between APs originating from different C-fibers, and estimates latency shifts and recovery constants quantitatively has been developed [10].

In this paper, we will present the analysis program with emphasis on the signal processing algorithms used. Many of these are based on previous algorithms [11] and are here further developed and analyzed.

II. Algorithm Overview

To study the characteristics of the latency time course, two major problems need to be solved: the detection of action potentials in noisy recordings and the discrimination of APs originating from different C-fibers.

Signal detection in noise is a problem with well-known solutions [12] and implementing the AP detector is straight-forward. The discrimination problem, on the other hand, presents an interesting challenge. We have found that a reliable algorithm may be derived by exploiting the marking phenomenon and tracking the APs of a particular C-fiber in the responses to the repetitive electrical stimulus, hence viewing the discrimination problem as a target tracking problem.

Once the time course of the latency corresponding to a particular C-fiber unit is isolated, a parametric model may be fitted to the data.

By merging these ideas, we obtain an approach that analyzes the C-fiber recordings in three steps, see Fig. 2:

1. *Detection* – Prior to any further processing, the action potentials must be detected. In our implementation, this is done by a matched filter (MF).

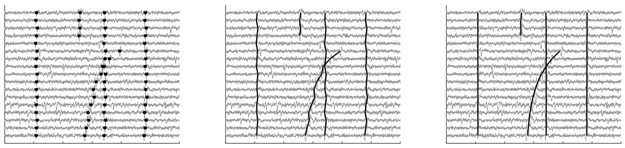

Fig. 2. Sample results from the three steps of the algorithm. Left: the APs are detected by the MF. Middle: the MHT algorithm is applied, resulting in five tracks. Right: the final trajectories are obtained by fitting a parametric model to the data.

2. *Tracking* – Once the action potentials are detected, the discrimination is carried out. Although the discrimination may be easy for an experienced analyst, it is a difficult problem to solve automatically using a computer. By regarding the assignment as a target tracking problem, we solve it using the multiple hypothesis tracking (MHT) method [13].
3. *Parameter estimation* – Following the tracking/discrimination step, the steady-state latency, the latency shift, and the recovery constant are estimated by fitting the latency model to the data. Currently, we use the simplex algorithm in combination with the least squares method.

This paper is organized as a description of the three main steps of the algorithm. Section III describes how the detection is done and how the optimal detector is derived. Section IV deals with the tracking of the APs using the MHT method and Kalman filtering, and describes how the AP amplitude is incorporated into the tracking algorithm. Section V describes the latency model and the parameter estimation. Section VI presents the characteristics and performance of the algorithms through simulations and theoretical analysis. Finally, Section VII illustrates the performance of the application on actual recordings obtained from awake human subjects.

III. Target Detection

Detecting signals hidden in high levels of noise is a delicate task. If the signal is a member of a set of signals with known shapes and if the color of the noise is known, then *matched filtering* constitutes a standard signal processing technique for optimally enhancing and detecting the signal [12]. Although these assumptions do not fully apply in this particular application, the performance provided by the MF is still good.

A. Matched filtering

Let the recorded discrete time data $\mathbf{z}(t)$ be hypothesized to take on one of the forms

$$H_0 : \mathbf{z}(t) = \boldsymbol{\eta}(t) \tag{1}$$

$$H_1 : \mathbf{z}(t) = \mathbf{s}(t) + \boldsymbol{\eta}(t) \tag{2}$$

where $\mathbf{z}(t)$, $\mathbf{s}(t)$, and $\boldsymbol{\eta}(t)$ constitute samples of the data, the (deterministic) signal, and the noise, respectively. They are all p-dimensional vectors defined as

$$\mathbf{z}(t) \triangleq \big(z(t) \ \ldots \ z(t-p+1)\big)^T \tag{3}$$

$$\mathbf{s}(t) \triangleq \big(s(t) \ \ldots \ s(t-p+1)\big)^T \tag{4}$$

$$\boldsymbol{\eta}(t) \triangleq \big(\eta(t) \ \ldots \ \eta(t-p+1)\big)^T \tag{5}$$

where ^{T} denotes the vector transpose. It is now assumed that the signal $\mathbf{s}(t)$ contains well-separated action potentials and that the noise $\boldsymbol{\eta}(t)$ has zero mean. As the APs are similar in shape but differ in amplitude, a p-dimensional *template* $\mathbf{s}$ and an *amplitude* γ are introduced to describe an AP present in the recording at a particular time of detection t_d

$$\mathbf{s}(t_d) = \gamma \mathbf{s}. \tag{6}$$

The objective is to determine whether there is an action potential $\mathbf{s}$ present or not in the measurement $\mathbf{z}(t)$. For a given matched filter impulse response

$$\mathbf{h} \stackrel{\triangle}{=} \begin{pmatrix} h(0) & h(1) & \dots & h(p-1) \end{pmatrix}^T \tag{7}$$

and the filter output

$$m(t) = \sum_{i=0}^{p-1} h(i) z(t-i) = \mathbf{h}^T \mathbf{z}(t) \tag{8}$$

the decision that the prescribed signal template $\mathbf{s}$ is present is made whenever $m(t_d)$ exceeds a given threshold level m_0 resulting in a maximum likelihood (ML) detector.

Assuming the noise to be white, the optimal impulse response $\mathbf{h}_o$ of the MF and the output signal-to-noise ratio SNR_{mf} may be calculated in terms of the known signal vector $\mathbf{s}$ and the noise variance σ^2 according to [12] [14]

$$\mathbf{h}_o = \frac{\mathbf{s}}{\sqrt{\sigma^2 \mathbf{s}^T \mathbf{s}}} \tag{9}$$

$$SNR_{mf} = \frac{\gamma^2}{\sigma^2} \mathbf{s}^T \mathbf{s}. \tag{10}$$

Combining (6) and (8)-(10), we obtain some interesting properties of this matched filter, namely

$$\begin{aligned} E\, m(t_d) &= \frac{\mathbf{s}^T}{\sqrt{\sigma^2 \mathbf{s}^T \mathbf{s}}} E(\mathbf{s}(t_d) + \boldsymbol{\eta}(t_d)) \\ &= \frac{\gamma \mathbf{s}^T \mathbf{s}}{\sqrt{\sigma^2 \mathbf{s}^T \mathbf{s}}} = \sqrt{SNR_{mf}} \qquad (11) \\ E\left(m(t_d) - \sqrt{SNR_{mf}}\right)^2 &= \frac{\mathbf{s}^T E(\boldsymbol{\eta}(t_d)\boldsymbol{\eta}^T(t_d))\mathbf{s}}{\sigma^2 \mathbf{s}^T \mathbf{s}} \\ &= \frac{\sigma^2 \mathbf{s}^T \mathbf{s}}{\sigma^2 \mathbf{s}^T \mathbf{s}} = 1 \qquad (12) \end{aligned}$$

where E is the expectation with respect to $\boldsymbol{\eta}(t)$. These relations will be utilized below to estimate the amplitude.

When the noise is not white, we proceed as described in Appendix A.

B. Detection performance

Using (8) and (9), and assuming that the noise $\boldsymbol{\eta}(t)$ is Gaussian, the MF output $m(t_d)$ is a stochastic variable having a Gaussian distribution with mean as described by (11) and with unit variance as described by (12). The false alarm probability P_{FA} and the detection probability P_D may thus be calculated by means of the decision threshold m_0 using the Gaussian distribution density function $\Phi(\cdot)$, see Fig. 3,

$$\begin{aligned} P_{FA} &= 1 - \Phi(m_0) \qquad (13) \\ P_D &= 1 - \Phi\left(m_0 - \sqrt{SNR_{mf}}\right). \qquad (14) \end{aligned}$$

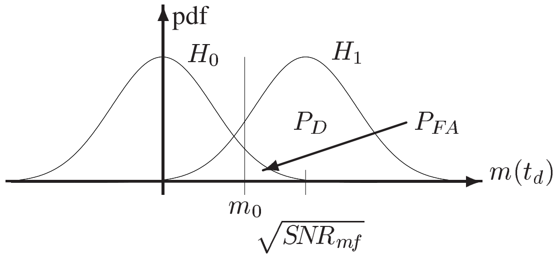

Fig. 3. This figure shows the probability density functions (pdf:s) of the two hypotheses. Under the hypothesis H_0, the data contains zero mean noise only and the corresponding pdf is centered around zero. Under the hypothesis H_1, the expectation of the MF output is equal to $\sqrt{SNR_{mf}}$ and the pdf is centered around that value. The false alarm probability P_{FA} and the detection probability P_D are equal to the area under their respective pdf above the detection threshold m_0, as shown in the figure.

The false alarm probability P_{FA} depends on the detection threshold m_0 only, meaning that the MF detector has a constant false alarm rate (CFAR). This is a desirable detector property in most applications.

C. Noise variance estimation

Because the noise variance is unknown and may change during the experiment, it has to be estimated from the recorded data. The recordings may, however, also contain hum from the power supply and surrounding equipment that yield a bias if not accounted for. By first removing the hum, using a notch filter, a simple variance estimator may be used.

Neglecting any APs and assuming the noise variance to be constant during the trace, the ML estimate of the noise variance $\hat{\sigma}^2$ is calculated using the notched data samples $w_n(t)$ in one trace of length N as

$$\hat{\sigma}^2 = \frac{1}{N} \sum_{t=0}^{N-1} w_n^2(t). \tag{15}$$

This is still a biased estimate,[2] but the bias decreases as the width of the notch decreases. As most practical cases regard a narrow notch filter, the influence of the bias may be neglected and is not considered further. Of more importance is the possible influence of the action potentials present in the recorded data. It is known from experience, however, that they only slightly contribute to the variance estimate.

Using the ML estimate (15) of the noise variance, the impulse response and the SNR of the matched filter are given by (9) and (10) with σ exchanged by $\hat{\sigma}$.[3]

D. Tuning

The basic assumption in deriving the matched filter is that the signal to be detected is known in advance. Although this is not the case here, it is known that the C-fiber action potentials are similar in shape and differ mainly by a scalar factor γ. It is

[2] Noise energy is of course removed and some hum energy is still present.

[3] Introducing the ML estimate of the variance formally implies that a Kelly test [14] should be used instead of the generalized likelihood ratio test (GLRT) used here. Moreover, the MF output then has a t-distribution instead of a normal distribution. However, the number of data points used in the estimations is so large that these effects have a negligible effect on the result.

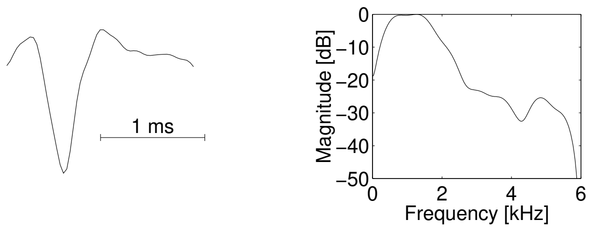

Fig. 4. The template of the C-fiber action potentials to be detected, i.e. the time-reversed impulse response of the matched filter (left), and the corresponding Bode magnitude plot (right).

thus possible to use any already recorded action potential as the template $\mathbf{s}$ to tune the matched filter.

To extract such a template from earlier recordings, several traces of good quality are aligned and averaged to reduce the influence of the noise and the background activity. Further reduction of the disturbances in the frequency region where no AP energy is expected is accomplished by low pass filtering the averaged potential. Fig. 4 shows the resulting signal template and the corresponding Bode plot.

E. Action potential detection

The sampling frequency used is 31.25 kHz and the spectral content of the APs is concentrated to the frequency range between 500 Hz and 1500 Hz. The matched filter constitutes an optimized bandpass filter with passband in this frequency range. The filter output is smooth and the time instants where APs are present may be obtained using a simple peak finding algorithm that reports all peaks above the given threshold m_0.

In Section VI-A the performance of this MF is analyzed in terms of resolution, variance, detection probability, and false-alarm probability.

IV. Target Tracking

Once the action potentials are detected, the APs corresponding to a particular C-fiber should be grouped together. This grouping could be done in various ways. If the shapes of the APs were different for different units, a bank of matched filters could be used for the grouping, where each matched filter would then be individually optimized to detect APs originating from one of the fibers only.

As mentioned in Section III, however, the action potentials are similar in shape so another method has to be used. Due to different conduction velocity in different units, the latency contains information about which APs originate from the same unit.

An experienced eye easily exploits this information in subsequent traces and forms tracks of APs that belong to each other. We try to mimic this by solving the association problem as a tracking problem.

Although the tracks may be found using the latency information only, the tracking performance is improved if more information is utilized. Despite the difference in shape is too small to be useful in the discrimination of the APs, the amplitude is in general different for APs originating from different C-fiber units.[4] For simplicity, the peak value of the matched filter output is used as an amplitude estimate. As may be seen from (11), this estimate is unbiased only if the recorded noise variance is constant over time. Although this is not necessarily true, the (biased) amplitude estimate has shown to perform well.

To solve the tracking problem, we have chosen the multiple hypothesis tracking (MHT) method, outlined next. An important part of this method is the target predictor. In the current implementation, we use a Kalman filter for a model derived in Section IV-B.

A. Multiple Hypothesis Tracking

Multiple hypothesis tracking (MHT) [15] is recognized as the theoretically best approach to multitarget tracking problems. In applications with heavy *clutter*[5] and high *traffic densities*,[6] the performance of MHT is outstanding compared to other methods, e.g. nearest neighbor (NN) correlation or joint probabilistic data association (JPDA) [16]. Therefore, we chose the MHT method for the current implementation.

A complete presentation of the MHT method is beyond the scope of this paper. However, since the current implementation is strongly influenced by the one presented by Blackman in [13], interested readers are directed to this book. The MHT parameters used and some of the few "tweaks" to the original work are presented in Appendix B.

The MHT method is a Bayesian probabilistic approach to the tracking problem. For each scan in the recorded data, the detected action potentials are collected by the tracking system. At a given time and with a given set of detected action potentials, there are several plausible ways to combine the APs into tracks. Instead of choosing only the most probable partitioning after each scan, the MHT method generates a number of candidate hypotheses to be evaluated later when more data are received. Thus, the probability of choosing the correct partitioning of the data into tracks and false alarms is increased.

To evaluate the probability of each hypothesis, a model of how the AP latencies change from scan to scan is needed. In Fig. 1 it may be seen that the latency is either constant or (approximately) exponentially decreasing. Both cases may be modeled by an exponential model. An expedient way to incorporate this model in the tracking method is the use of a Kalman filter, presented in Section IV-B.

The drawback of MHT is that the number of computations and the memory requirements are extensive. In our application, this is of less concern as the tracking is performed off-line. Furthermore, the requirements may be held at a reasonable level by limiting the number of hypotheses evaluated. There are several methods available for this, and three of them (gating, clustering, and pruning) are used here. This technique works well for the present application.

In Fig. 5 a block diagram of the MHT algorithm is presented. For each trace, the controlling logic iterates over the current

[4] The difference in amplitude of different C-fiber units could be explained by the different distances between the recording electrode and the nerve fibers.

[5] The term *clutter* is used for detections that are of no interest to the operator and that often degrade the performance of the tracking system. In radar surveillance contexts, for example, clutter is primarily used for ground echoes. In our context, clutter would be spurious APs and false detections that are uncorrelated with other APs.

[6] In our case, high *traffic densities* means that different C-fibers have very similar latencies.

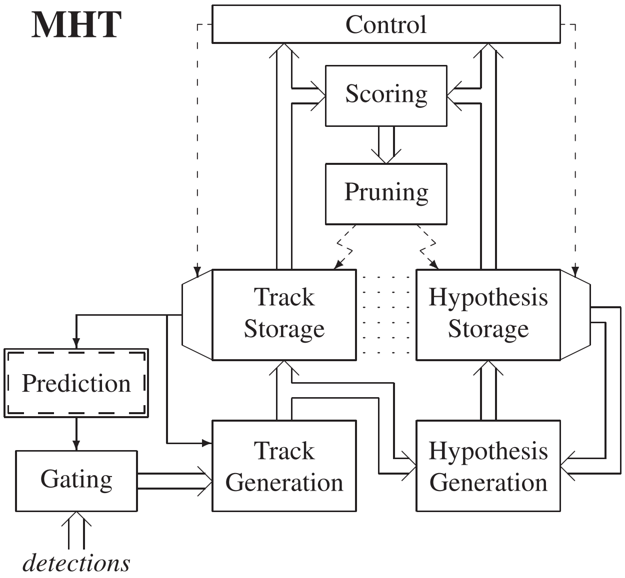

Fig. 5. A block diagram of the MHT algorithm. Data flow is indicated by solid lines; thin for single data and thick for multiple data. Control flow is indicated by dashed lines whereas other intimate relations are indicated by dotted lines.

track set. The track currently selected is fed to the predictor where the expected latency and the expected amplitude are calculated. A *gate* is formed around the prediction and all detections (in the current trace) that fall outside the gate are discarded. The current track and the gated detections are used by the track generator to both create updates of the track and to create entirely new tracks. The tracks produced by the track generator are then fed to the hypothesis generator as well as stored for use when processing the detections of the next trace.

At the same time as the current track was selected, the control logic also selected all hypotheses containing that track. These hypotheses are used together with the generated tracks to form updated hypotheses. The generated hypotheses are then stored in the hypothesis storage.

When the track iteration is completed, the *scores*[7] of all hypotheses are calculated and used to *prune* hypotheses (and tracks) associated with a low score. The process is then repeated for the detections in the next trace.

Note that the MHT algorithm does not depend on a particular predictor. The same algorithm may, in principle, be used for any tracking problem. Only the predictor needs to be changed.

Since the computation complexity grows exponentially with the number of tracks, the most effective way to reduce it is to separate non-interacting hypotheses into independent *clusters* [17] [15] (not shown in Fig. 5). Instead of solving one large tracking problem, a number of smaller tracking problems are then solved separately.

B. Kalman Filter

From the presentation above, it is clear that fundamental in any tracking system is the track prediction and filtering. The two major alternative methods used today are the Kalman filter [18] and the filter based on interacting multiple models (IMM) [19]. The IMM method is an extension of the multiple model (MM) approach [20] [21] to handle model switching and often provides the best performance. However, the IMM method is suboptimal and in the application under consideration no model switches occur, which suggests that the MM method would give the best performance. At present, the Kalman filter is used, but extending this to an MM based filtering method is straightforward, if required.[8]

As the process under study is a real physical process assumed to be working in continuous time, a model is based on this assumption. To incorporate such a model in the tracking process, a discrete time model is produced by sampling the continuous time model. The measurements, however, are modeled as a discrete time process directly. Prior to the presentation of the discrete time models, a description of the underlying continuous time model will be given.

B.1 The continuous time model

From Fig. 1 it seems reasonable to assume that the measured latency, denoted $y_1(t)$, may be modeled by

$$y_1(t) \triangleq \bar{y}_1(t) + \varepsilon(t) \tag{16}$$
$$\bar{y}_1(t) \triangleq y_0 + Ae^{-\alpha_0(t-t_0)}, \quad t \geq t_0 \tag{17}$$

where $\bar{y}_1(t)$ is the *true* but unknown latency, y_0 is the latency at steady state, A is the latency shift due to stimulation, α_0 is the recovery coefficient, t_0 is the time of excitation, and $\varepsilon(t)$ is the residual or model error. By selecting the true latency $\bar{y}_1(t)$ and its derivative $\dot{\bar{y}}_1(t)$ as state variables, (17) may be written in state space form as

$$\begin{pmatrix} \dot{\bar{y}}_1(t) \\ \ddot{\bar{y}}_1(t) \end{pmatrix} = \begin{pmatrix} 0 & 1 \\ 0 & -\alpha_0 \end{pmatrix} \begin{pmatrix} \bar{y}_1(t) \\ \dot{\bar{y}}_1(t) \end{pmatrix}, \quad t \geq t_0 \tag{18}$$
$$\bar{y}_1(t_0) = y_0 + A \tag{19}$$
$$\dot{\bar{y}}_1(t_0) = -\alpha_0 A \tag{20}$$

which is an initial value problem with (17) as its solution. It is simple to augment this deterministic state space model with an additional state that describes the action potential amplitude assumed to be constant.

To account for errors in the unknown parameter α_0 and slow variations in the latency and the AP amplitude, it is conventional to add noise terms to the uncertain states.[9] The *deterministic* continuous time state space model (18) augmented with the AP amplitude is thus replaced by a *stochastic* continuous time state

[7]The hypothesis *score* is the logarithm of the a posteriori probability of that hypothesis being correct so scaled that an all-false-alarm hypothesis has a zero score.

[8]In the MM approach a bank of prediction filters, e.g. Kalman filters, are mixed to cover a broader range of target models. Using a single Kalman filter is therefore identical to a MM approach with a single model.

[9]A thorough presentation of these concepts is given in [20].

space model[10]

$$\mathbf{dx}_c(t) \;=\; \mathbf{A}\mathbf{x}_c(t)\,dt + \mathbf{G}\,\mathbf{dw}(t), \quad t \geq t_0 \tag{21}$$

$$\mathbf{A} \;\triangleq\; \begin{pmatrix} 0 & 1 & 0 \\ 0 & -\alpha & 0 \\ 0 & 0 & 0 \end{pmatrix} \tag{22}$$

$$\mathbf{G} \;\triangleq\; \begin{pmatrix} 0 & 0 \\ 1 & 0 \\ 0 & 1 \end{pmatrix} \tag{23}$$

where $\mathbf{x}_c(t)$ is the three-dimensional continuous time state vector consisting of the latency $\bar{y}_1(t)$, its derivative $\dot{\bar{y}}_1(t)$, and the square root of the SNR at the matched filter output SNR_{mf} (equal to the *true* MF output, see (11)). The square root of the SNR is used because it is proportional to the amplitude of the action potential detected and has a direct relation with the matched filter peak value. The two-dimensional entity $\mathbf{dw}(t)$ is the *Wiener increment* [22] of a two-dimensional Wiener process $\mathbf{w}(t)$. The matrix $\mathbf{A}$ is the state transition matrix, in which α should be as close as possible to the true recovery coefficient α_0. Note that the limit $\alpha = 0$ results in the common first order white noise acceleration model described in [20].

Because the latency modeling errors are largest at the start of the decay and are almost zero at steady state, the incremental variance of $dw_1(t)$ (the first element of $\mathbf{dw}(t)$) is defined as

$$\begin{aligned} \sigma^2_{e_1}(t)\,dt \;&\triangleq\; E\,(dw_1(t))^2 \\ &=\; \sigma^2_{e_1}(1 + e^{\beta_0 - \beta_1(t-t_0)})\,dt, \quad t \geq t_0 \end{aligned} \tag{24}$$

where β_i are tuning parameters. This results in a process noise that is high at onset and decreases exponentially to its minimum. Note that this affects the latency part of the system only. For the modeling of the amplitude estimate, a constant incremental variance $\sigma^2_{e_2} dt$ is used.

Consequently, the incremental covariance matrix $\Lambda(t)\,dt$ of the Wiener increment $\mathbf{dw}(t)$ is given by

$$\Lambda(t)\,dt \triangleq E\,\mathbf{dw}(t)\mathbf{dw}^T(t) = \begin{pmatrix} \sigma^2_{e_1}(t) & 0 \\ 0 & \sigma^2_{e_2} \end{pmatrix} dt. \tag{25}$$

B.2 The discrete time model

The utilization of the marking phenomenon, i.e. emitting electrical impulses periodically and measuring the latency of the evoked APs, may be interpreted as a sampling of the (continuous time) latency of the excited units with a sampling interval equal to the period of the emitted stimuli. The time difference between the emission of the impulse and the detection of the evoked AP of a particular C-unit is then a measurement of the current latency of this unit. Any additional APs manifest themselves by increased time differences corresponding to an increased C-unit latency in accordance with the marking phenomenon.[11]

By sampling the continuous time model we obtain the process model in trace k

$$\mathbf{x}(k+1) \;=\; \mathbf{F}\mathbf{x}(k) + \mathbf{v}_1(k), \quad k \geq k_0 \triangleq \frac{t_0}{T} \tag{26}$$

$$\mathbf{x}(k) \;\triangleq\; \mathbf{x}_c(kT) \tag{27}$$

$$\mathbf{F} \;\triangleq\; e^{\mathbf{A}T} = \begin{pmatrix} 1 & \alpha^{-1}(1-e^{-\alpha T}) & 0 \\ 0 & e^{-\alpha T} & 0 \\ 0 & 0 & 1 \end{pmatrix} \tag{28}$$

$$\mathbf{v}_1(k) \;\triangleq \int_0^T e^{\mathbf{A}(T-\tau)}\mathbf{G}\,\mathbf{dw}(kT+\tau) \tag{29}$$

$$\mathbf{Q}_1(k) \;\triangleq\; E\,\mathbf{v}_1(k)\mathbf{v}_1^T(k) \tag{30}$$

where T is the period of the repetitive electrical stimulation and the transition matrix $\mathbf{F}$ describes the discrete time system dynamics and is derived via the series expansion $e^{\mathbf{A}T} = \mathbf{I} + \mathbf{A}T + \frac{1}{2!}(\mathbf{A}T)^2 + \ldots$ [23]. The three-dimensional vector $\mathbf{v}_1(k)$ represents process noise[12] modeled as zero-mean, white-noise Gaussian processes with covariance matrix $\mathbf{Q}_1(k)$ derived in Appendix C.

B.3 Measurement model

The measurement model describes how the measurements are collected and is defined as

$$\mathbf{y}(k) \;=\; \mathbf{H}\mathbf{x}(k) + \mathbf{v}_2(k) \tag{31}$$

$$\mathbf{H} \;\triangleq\; \begin{pmatrix} 1 & 0 & 0 \\ 0 & 0 & 1 \end{pmatrix} \tag{32}$$

where $\mathbf{y}(k)$ is a two-dimensional measurement vector containing the latency and the matched filter peak output. The two-dimensional vector $\mathbf{v}_2(k)$ is the measurement noise, modeled as independent zero-mean white-noise Gaussian processes with a known constant $2|2$ covariance matrix

$$\mathbf{Q}_2 \triangleq E\,\mathbf{v}_2(k)\mathbf{v}_2^T(k) = \begin{pmatrix} q^{(2)}_{11} & 0 \\ 0 & q^{(2)}_{22} \end{pmatrix}. \tag{33}$$

B.4 Kalman filter algorithm

Assuming the state space model (26)-(33) describes the true system correctly, the Kalman filter provides the optimal mean-squared error estimate $\hat{\mathbf{x}}(k|k)$ and the one-step prediction $\hat{\mathbf{x}}(k+1|k)$ according to

$$\tilde{\mathbf{y}}(k) \;=\; \mathbf{y}(k) - \mathbf{H}\hat{\mathbf{x}}(k|k-1) \tag{34}$$

$$\mathbf{S}(k) \;=\; \mathbf{H}\mathbf{P}(k|k-1)\mathbf{H}^T + \mathbf{Q}_2 \tag{35}$$

$$\mathbf{K}_f(k) \;=\; \mathbf{P}(k|k-1)\mathbf{H}^T\mathbf{S}^{-1}(k) \tag{36}$$

$$\hat{\mathbf{x}}(k|k) \;=\; \hat{\mathbf{x}}(k|k-1) + \mathbf{K}_f(k)\tilde{\mathbf{y}}(k) \tag{37}$$

$$\hat{\mathbf{x}}(k+1|k) \;=\; \mathbf{F}\hat{\mathbf{x}}(k|k) \tag{38}$$

$$\mathbf{P}(k|k) \;=\; (\mathbf{I} - \mathbf{K}_f(k)\mathbf{H})\mathbf{P}(k|k-1) \tag{39}$$

$$\mathbf{P}(k+1|k) \;=\; \mathbf{F}\mathbf{P}(k|k)\mathbf{F}^T + \mathbf{Q}_1(k) \tag{40}$$

where $\mathbf{I}$ is the $3|3$ identity matrix, $\tilde{\mathbf{y}}(k)$ is the measurement prediction error, called the *innovation*, and $\mathbf{K}_f(k)$ is the Kalman

[10] The stochastic differential equation (21) may be interpreted as $\dot{\mathbf{x}}_c(t) = \mathbf{A}\mathbf{x}_c(t) + \mathbf{G}\mathbf{e}(t)$, where $\mathbf{e}(t)$ is a two-dimensional continuous time white noise process.

[11] The "sampling" impulses do, of course, increase the latency in exactly the same way as other stimuli that evoke APs. The latency will stabilize at an equilibrium, however, where the latency increase and the unit recovery will cancel each other. Therefore, these "sampling" effects may be incorporated into the steady state latency y_0.

[12] In equation (29), the entity $\mathbf{dw}(kT+\tau)$ may be interpreted as $\mathbf{e}(kT+\tau)d\tau$, where $\mathbf{e}(t)$ is a two-dimensional continuous time white noise process.

filter gain. The 3|3 matrix $\mathbf{P}(k|k)$, $\mathbf{P}(k+1|k)$, and the 2|2 matrix $\mathbf{S}(k)$ are the filter error, the one-step prediction error, and the measurement prediction error covariance matrices, respectively. They are defined as

$$\tilde{\mathbf{x}}(k+1|k) \triangleq \mathbf{x}(k+1) - \hat{\mathbf{x}}(k+1|k) \tag{41}$$

$$\mathbf{P}(k+i|k) \triangleq E\,\tilde{\mathbf{x}}(k+i|k)\tilde{\mathbf{x}}^T(k+i|k), \quad i = 0,1 \tag{42}$$

$$\mathbf{S}(k) \triangleq E\,\tilde{\mathbf{y}}(k)\tilde{\mathbf{y}}^T(k). \tag{43}$$

B.5 Initiation

Before the use of the recursion (36)-(40), initial estimates of the state and its covariance matrix need to be found. An LS estimate using two measurements is presented in Appendix D.

B.6 Consistency

Despite the robustness (in terms of the MSE) of the Kalman filter, it could be well worth the effort checking the consistency of the filter. The consistency analysis as described in [20] provides a good insight that is valuable when deriving and tuning the filter model. For the Kalman filter to provide consistent estimates, the following conditions have to be fulfilled:
1. The filter is unbiased, i.e. the state errors are zero mean.
2. The filter calculated covariance matrices are equal to the covariance matrices of the actual state and measurement errors.
3. The innovations are zero mean and white.
4. The initial state and its covariance matrix are set to their expectations.

V. Parameter Estimation

The model function $\bar{\mathbf{y}}(\boldsymbol{\theta})$ and the data $\mathbf{y}$ are defined by

$$\bar{\mathbf{y}}(\boldsymbol{\theta}) = \left(\bar{y}_1(k_0,\boldsymbol{\theta}) \ \ldots \ \bar{y}_1(k_{N-1},\boldsymbol{\theta}) \right)^T \tag{44}$$

$$\mathbf{y} = \left(y_1(k_0) \ \ldots \ y_1(k_{N-1}) \right)^T \tag{45}$$

$$\bar{y}_1(k,\boldsymbol{\theta}) = y_0 + Ae^{-\alpha(k-k_0)T}, \quad k \in K \tag{46}$$

$$\boldsymbol{\theta} \triangleq \left(\alpha \ y_0 \ A \right)^T \tag{47}$$

$$K \triangleq \{k_0,\, k_1,\, \ldots,\, k_{N-1}\} \tag{48}$$

where $\bar{y}_1(k,\boldsymbol{\theta})$ is a parametrized model of the latency defined in accordance with the assumed time course of the latency in (17). Each element $y_1(k_i)$ is the measured latency (the first element of the measurement vector $\mathbf{y}(k_i)$) of the AP assigned to this track in trace number k_i. The set K contains all trace numbers for which an AP has been assigned to this track and N is the number of assignments.

The set of (nonlinear) regression equations may then be written

$$\mathbf{y} = \bar{\mathbf{y}}(\boldsymbol{\theta}) + \boldsymbol{\varepsilon} \tag{49}$$

where $\boldsymbol{\varepsilon}$ is an N-dimensional residual column vector. This system of equations is solved to find the parameter estimate $\hat{\boldsymbol{\theta}}$ that minimizes the squared sum of the residual $\boldsymbol{\varepsilon}$.

In the model (46) the parameter α enters nonlinearly, whereas the two parameters y_0 and A enter linearly. The parameters is estimated by an iterative method in which the nonlinear term is estimated using the simplex method [24] [25]. For each step in the simplex algorithm, the two linear terms are estimated through the least squares method and the error norm is returned. The simplex method thus seeks the parameter α through

$$\hat{\alpha} = \arg\min_{\alpha} \sum_{k\in K} \left| y_1(k) - \bar{y}_1(k,\alpha|\hat{y}_0,\hat{A}) \right|^2. \tag{50}$$

The two linear terms $\hat{y}_0$ and $\hat{A}$ are estimated with the least squares method by solving the over-determined system of equations

$$\mathbf{J}_{lin}(\alpha) \begin{pmatrix} \hat{y}_0 \\ \hat{A} \end{pmatrix} = \mathbf{y} \tag{51}$$

where $\mathbf{J}_{lin}$ is found by deriving the Jacobian [26] of the parametrized model. The Jacobian is defined by

$$\mathbf{J}(\boldsymbol{\theta}) \triangleq \frac{\partial}{\partial \boldsymbol{\theta}^T}\bar{\mathbf{y}}(\boldsymbol{\theta}) = \left(\mathbf{j}_\alpha(\alpha,A) \ \ \mathbf{J}_{lin}(\alpha) \right) \tag{52}$$

$$\mathbf{j}_\alpha(\alpha,A) = \begin{pmatrix} 0 \\ -(k_1-k_0)TAe^{-\alpha(k_1-k_0)T} \\ \vdots \\ -(k_{N-1}-k_0)TAe^{-\alpha(k_{N-1}-k_0)T} \end{pmatrix} \tag{53}$$

$$\mathbf{J}_{lin}(\alpha) = \begin{pmatrix} 1 & 1 \\ 1 & e^{-\alpha(k_1-k_0)T} \\ \vdots & \vdots \\ 1 & e^{-\alpha(k_{N-1}-k_0)T} \end{pmatrix}. \tag{54}$$

The initial value of the recovery constant α is set to the slope coefficient of the linear regression of the data.[13]

In [27], confidence intervals of the estimates are derived for a parametrized vector function $\bar{\mathbf{y}}(\boldsymbol{\theta}_0)$ where $\boldsymbol{\theta}_0$ represents the true parameter vector. Given a parameter estimate $\hat{\boldsymbol{\theta}}$ and some scalar function $\phi(\boldsymbol{\theta})$, a confidence interval I_p with confidence level $1-p$ of the scalar $\phi(\boldsymbol{\theta}_0)$ is[14]

$$I_p = \{\phi(\boldsymbol{\theta}) \mid P(\phi(\boldsymbol{\theta}_0) \in I_p) = 1-p\} \tag{55}$$

$$= \left[\phi(\hat{\boldsymbol{\theta}}) \pm t_{N-3;1-p/2}\sqrt{s^2\hat{\Phi}\hat{\mathbf{C}}\hat{\Phi}^T}\right] \tag{56}$$

$$\hat{\mathbf{C}} \triangleq \left(\mathbf{J}^T(\hat{\boldsymbol{\theta}})\mathbf{J}(\hat{\boldsymbol{\theta}})\right)^{-1} \tag{57}$$

$$\hat{\Phi} \triangleq \left.\frac{\partial}{\partial \boldsymbol{\theta}^T}\phi(\boldsymbol{\theta})\right|_{\boldsymbol{\theta}=\hat{\boldsymbol{\theta}}} \tag{58}$$

$$s^2 = \frac{1}{N-3}\left(\mathbf{y}-\hat{\mathbf{y}}(\hat{\boldsymbol{\theta}})\right)^T\left(\mathbf{y}-\hat{\mathbf{y}}(\hat{\boldsymbol{\theta}})\right) \tag{59}$$

where $t_{N-3;1-p/2}$ denotes the upper $1-p/2$ critical point of the t-distribution with $N-3$ degrees of freedom. The confidence interval of the estimates is thus calculated as

$$I_p^{(y_0)} = \hat{y}_0 \pm t_{N-3;1-p/2}\sqrt{s^2\hat{c}_{11}} \tag{60}$$

$$I_p^{(A)} = \hat{A} \pm t_{N-3;1-p/2}\sqrt{s^2\hat{c}_{22}} \tag{61}$$

$$I_p^{(\alpha)} = \hat{\alpha} \pm t_{N-3;1-p/2}\sqrt{s^2\hat{c}_{33}} \tag{62}$$

[13] This results in a good initial estimate for short (with respect to the recovery constant) data sets, but has the drawback of yielding worse estimates for long data sets.

[14] Note that the matrix $\hat{\mathbf{C}}$ may be badly conditioned and that the columns in $\mathbf{J}(\hat{\boldsymbol{\theta}})$ could need a rescaling.

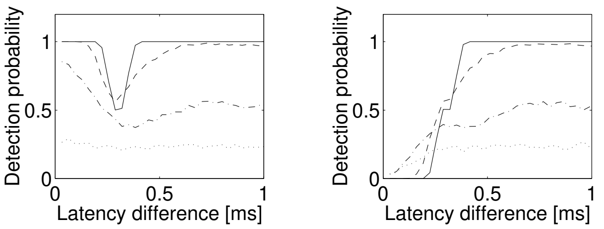

Fig. 6. The estimated detection probabilities as a result of 1000 Monte Carlo simulations where two action potentials with different latencies are detected ($m_0 = 1$) at different signal-to-noise ratios, -20 dB (dotted), 0 dB (dash dotted), 10 dB (dashed), and 20 dB (solid). The detection assignments were made in favor of the first AP (left). For small latency differences, the APs may not be resolved and the detection probability of the second AP (right) drops to zero. This result suggests that the MF detection resolution is 0.4 ms.

where $\hat{c}_{ii}$ are the diagonal elements of $\hat{\mathbf{C}}$ in (57). Unfortunately, the theory is valid only asymptotically and the above confidence intervals are too large for the relatively short track segments used in the application at hand.

VI. Simulation Results

Below, simulations are presented for the matched filter as its properties are essential to the tuning of the Kalman filter and affect the tuning of the MHT algorithm. The consistency analysis of the Kalman filter is not included due to its limited value to the presentation of this paper. It is, however, an important tool when tuning the Kalman filter, see Section VII-B.1 and [20] for details.

A. The matched filter detector

Throughout the simulations of the matched filter, 1000 Monte Carlo runs were done with the detection threshold set to $m_0 = 1$.

A.1 Resolution

An important property of the MF detector is its resolution capability because this is a term in the false-target intensity parameter of the tracker. Moreover, the resolution characteristics influences the necessary MHT performance on crossing tracks.

To estimate the detection probability as a function of the time difference between two close APs, the number of detections within an interval centered around the expected detection point were calculated. The length of the interval was a third of the width of the main peak in the auto-correlation function of the signal template (0.3 ms).

If several detections were made within the interval, the detection time closest to the one expected was chosen. If, at small time differences, the two APs competed for the same detection, the detection count was assigned to the first AP.

Fig. 6 shows the detection probability of two crossing targets at different SNRs. As expected, the detection probability of the second AP decreases to zero for small time differences. The detection probability of the first AP increases instead, because the APs add and interfere constructively. Surprisingly, there is a dip in the detection probability between 0.2 ms and 0.4 ms (for both APs) where the two APs interfere destructively with one another. From this, we conclude that the tracker should be robust with respect to changes in the detection probability at track crossings. If not, tracks may be lost or swapped.

For the high SNR case (20 dB), the detection probability of the second AP is unity for large time differences and drops sharply to zero when the time difference is less than 0.4 ms. This suggests that the detection resolution of the MF detector is

$$\Delta_{lat} = 0.4 \quad [\mathrm{ms}]. \tag{63}$$

A.2 Detection and false alarm probability

In several of the equations constituting the MHT algorithm, the detection and false alarm probabilities are key parameters. Theoretical expressions were presented in Section III-B assuming the position of the signal is known, i.e. the MF only detects whether the signal is *present*, not *where* it is.

This assumption, however, does not hold in this application. Instead, whenever the MF output peaks and exceeds the current threshold, a signal is assumed to be present at the peak location. This may make a difference to the theoretically calculated probabilities, and in this section, the detection and false alarm probabilities are estimated as functions of the SNR levels and compared to the theoretical values.

The simulation results in Fig. 7 show that the estimated detection and false alarm probabilities are within the 95% confidence intervals except for the detection probability at low SNRs. This discrepancy is expected because the implementation above takes advantage of the correlation in the MF output. For example, if the MF output at the expected latency is just below the threshold, it may be above the threshold in a neighboring sample where a detection would be reported. Thus, the actual detection probability is increased compared with the theoretical value for low SNR levels.

When calculating the false alarm probability, the correlation of the MF output has to be considered. Experience has shown that the false alarm probability P_{FA} may successfully be estimated through

$$\widehat{P}_{FA} \triangleq \frac{n}{N}\frac{\Delta_{lat}}{2L} \tag{64}$$

where n is the number of erroneous detections, N is the number of Monte Carlo runs, and L is the length of the interval.

A.3 Accuracy

To tune the Kalman filter properly, it is important to know the variance of the latency measurements, i.e. the accuracy of the MF detector.

As stated in Section III-E, the latency is found by searching for peaks in the MF output. Because the APs are unsynchronously sampled continuous time signals, the peaks in the MF output are also unsynchronous to, and not aligned with, the sampling instants. Moreover, the variance of the latency is expected to be just a few sampling periods and so the sample period quantization may not be neglected.

Because of this, the resolution of the latency measurements has to be increased before estimating the latency variance. For this, it was considered sufficient to oversample the MF output 10 times (interpolation). Also, the MF impulse response was first shifted a fraction of a sample period to locate its “time continuous peak” at a sample instant. When viewing histograms of

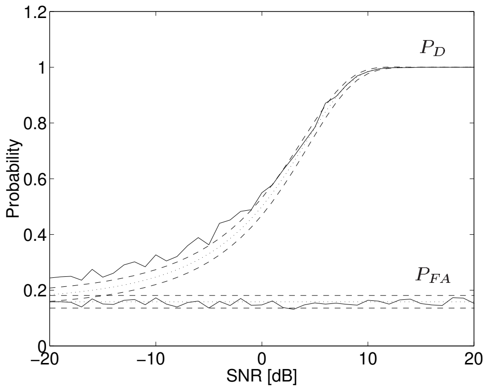

Fig. 7. The figure shows the estimated detection and false alarm probabilities from 1000 Monte Carlo simulations as a function of the SNR. The theoretical values are shown (dotted) as well as the 95% confidence regions (dashed). As clearly shown, the results correspond well to the theoretical probabilities except for the detection probability at low SNR levels. By taking advantage of the MF output correlation, the MF detector increases the resulting detection probability slightly. The MF threshold used is $m_0 = 1$.

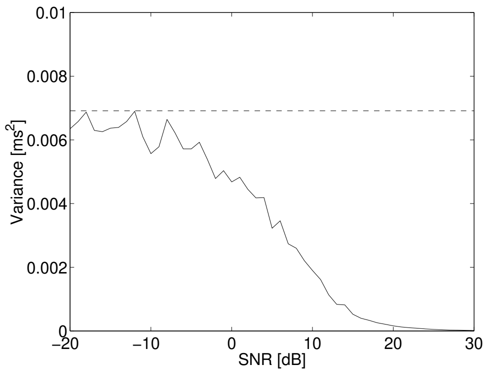

Fig. 8. The figure shows the estimated variance (solid) of the detection latencies from 1000 Monte Carlo simulations where the MF output has been oversampled ten times prior to the detection. For decreasing SNR levels, the variance increases asymptotically towards the variance of a uniform distribution over the detection interval (dashed).

the latency errors, it seemed reasonable, for high SNR levels, to assume that they were Gaussian and zero mean.

As Fig. 8 shows, the variance is small for high SNRs and increases when the SNR decreases. As expected, the variance approaches the variance of a uniform distribution over the simulated interval.

VII. Experimental Results

As stated in the introduction, the objective of the application is to detect low amplitude action potentials, combine them into tracks, and estimate the latency shift parameters and the recovery constants.

In this section, the performance of these three steps when applied to real recordings from human subjects is illustrated. First, it is made clear that the MF output has an improved detection capability compared to the original recording. Following that, the performance of the MHT tracker is illustrated in two different scenarios, one simpler and one harder. Finally, the estimated parameters of one of the active units found by the tracker are given.

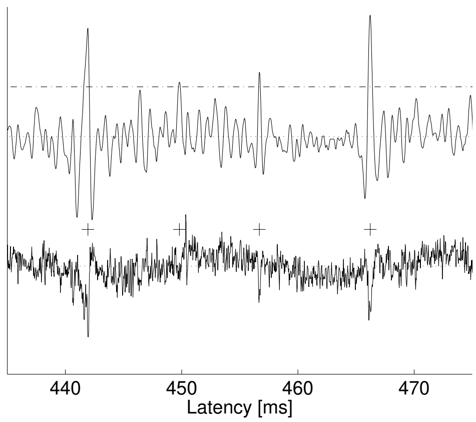

Fig. 9. The output of the matched filter (top) when applied on a part of scan 5 in the recording in Fig. 11 (bottom). With the same threshold setting, four detections are reported (+). Note also the 50 Hz hum in the recorded data.

A. The matched filter

Previously, a non-linear filter was used [28] to aid the detection of the APs in noisy recorded data. It is called a “noise-cut” filter, because it amplifies only the part of a signal that is above a certain magnitude and thus removes the middle, noisy portion of the signal.

The noise-cut filter works well for larger spikes, but has the drawback of not being useful when the APs are of the same order of magnitude as that of the noise itself. To achieve better performance, the matched filter has to detect APs of the same magnitude as the noise.

In Fig. 9 a part of the fifth scan in Fig. 11 is shown. As may be seen from Fig. 9, the matched filter output is an improvement to the original data. With the detections from several scans (see Fig. 11), it may be concluded that the four reported peaks (marked with +) could correspond to four AP detections and that even the low amplitude APs is detected without decreasing the detection threshold down to the noise level.

From Fig. 9 it is clear that a notch filter must be used to remove the 50 Hz hum in order to avoid a biased noise variance estimate (15).

B. Multiple hypotheses tracking

The most critical part of the overall system is the tracking of the different C-units. For this application to be useful, the number of tracking errors has to be small. Some errors are allowed because erroneous assignments may be corrected manually prior to the statistical analysis.

B.1 A two unit recording

This basic example involves two well-separated units, one with high and one with low amplitude, see Fig. 10. First, both units are inactive and their latencies are constant at about 303 ms and 360 ms, respectively. At scan 13, the high amplitude unit is activated by a mechanical stimulus and its latency increases dramatically. The latency then slowly recovers to the level before the activation.

As shown in Fig. 10, the algorithm is able to track all of the APs originating from the high amplitude unit and most of the

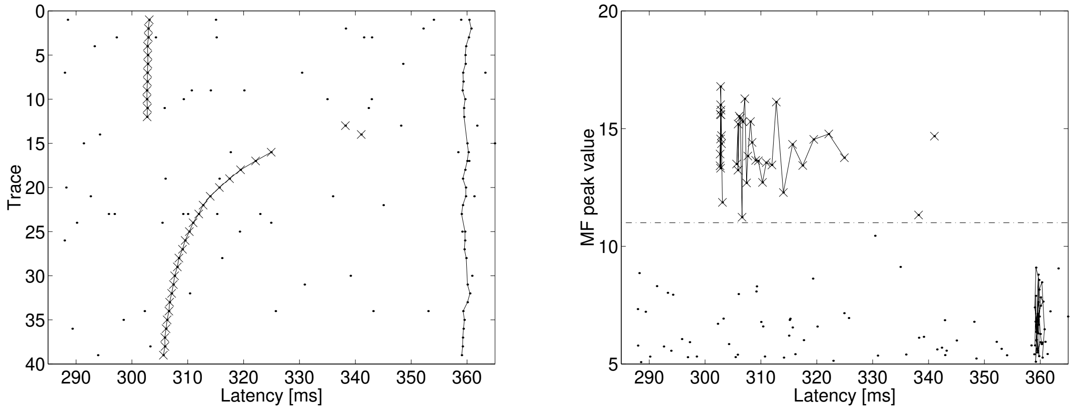

Fig. 10. The figure shows the confirmed tracks of the tracker when applied to the two C-fiber unit recording in Fig. 1. The two perspectives show the time course of the latencies of the units (left) and the amplitude information of the detected APs where the difference between the two units is clearly seen (right). The APs with an MF peak output above 11 (dash-dotted, right) are marked (x). For comments on the two marked APs in trace 13 and 14, see the text.

APs originating from the low amplitude unit. The detection threshold is set to $m_0 = 5$. Note that the track of the low amplitude unit is not lost even though its SNR is only slightly above the noise level.

Note also the two hig amplitude AP detections in trace 13 and 14 not assigned to any track. They probably originate from the high amplitude unit, but because they are found in the traces directly after activation of the unit, it is not clear whether they correspond to the electrical impulses, the mechanical stimulus, or some spurious after effects of the mechanical stimulus.

If only the high amplitude unit is of interest, the tracking may be simplified by choosing a higher threshold. For example, using $m_0 = 11$, only the x-marked APs in the diagrams of Fig. 10 would be detected and processed.

The good result despite the low threshold is a strength that is important in more complex situations.

To tune the Kalman filter settings appropriately, the parameters of the active unit's recovery trajectory were estimated, see Table I. Using the consistency analysis described in Section IV-B.6 and [20], the Kalman filter was subjectively tuned to give as consistent estimates as possible. The chosen parameters were

$$\begin{array}{rcll rcll}
\alpha &=& 0.0375 & [\mathrm{ms}^{-1}] & \beta_1 &=& 0.05 & [\mathrm{ms}^{-1}] \\
\sigma_{e_1}^2 &=& 2\cdot 10^{-5} & [\mathrm{ms}^{-1}] & q_{11}^{(2)} &=& 0.05 & [\mathrm{ms}^2] \\
\sigma_{e_2}^2 &=& 10^{-7} & [\mathrm{ms}^{-1}] & q_{22}^{(2)} &=& 1 & \\
\beta_0 &=& 3 & & & & &
\end{array} \quad (65)$$

Note that $q_{11}^{(2)}$ was selected larger than the variance of the residuals in Table I. This partly accounts for the non-Gaussian residuals and improves the consistency somewhat. Note that the filter is still not consistent with the data. This is, however, the best we may expect without reworking the Kalman filter.

B.2 A multi-unit recording

A more complex and more realistic example will now be presented, where several C-units are recorded and have crossing trajectories. Several of the units are inactive during the recording, and one of the units (drawn with a thick line) is strongly activated between scan 11 and scan 12, see Fig. 11. Moreover, there are two spontaneously active sympathetic C-units that may be recognized by their more irregular behavior.

It is evident from Fig. 11 that a good tracking result is obtained for the activated unit as well as for the inactive ones. In this example, no parameter estimation was done to tune the algorithms. Instead, the algorithm parameters are identical to the ones used in the previous example.

Moreover, the importance of the amplitude information should be obvious as the latency trajectory of the active unit crosses the two sympathetic units, but their amplitudes differ.

Note also the tracker's ability to discriminate between the two tracks at about 440 ms (trace 20-30) despite their closeness and low SNR levels.

Note, finally, the lost track between trace 45 and 46 (latency 440 ms). This tracking error may, however, be corrected by the operator before the parameter estimation is done.

C. Parameter estimation

Fitting an exponential curve to the active unit's trajectory in Fig. 10 results in the parameter and confidence intervals presented in Table I. As stated in Section V, the confidence intervals are too large. With this in mind, the relatively small confidence intervals presented in the table suggest that the parameter estimation procedure is accurate.

TABLE I

PARAMETER ESTIMATION OF THE ACTIVE UNIT IN FIG. 10. NOTE THAT THE RESIDUALS ARE NEITHER WHITE NOR GAUSSIAN.

Parameter		*Value*	*Conf. interval*
y_0	[ms]	305.4	$[305.1, 305.7]$
A	[ms]	19.44	$[19.06, 19.82]$
α	$[\mathrm{ms}^{-1}]$	0.0390	$[0.0369, 0.0411]$
s^2	$[\mathrm{ms}^2]$	0.026	N/A

VIII. DISCUSSION

An application of matched filtering and multiple hypothesis tracking applied to human nerve C-fiber action potentials was

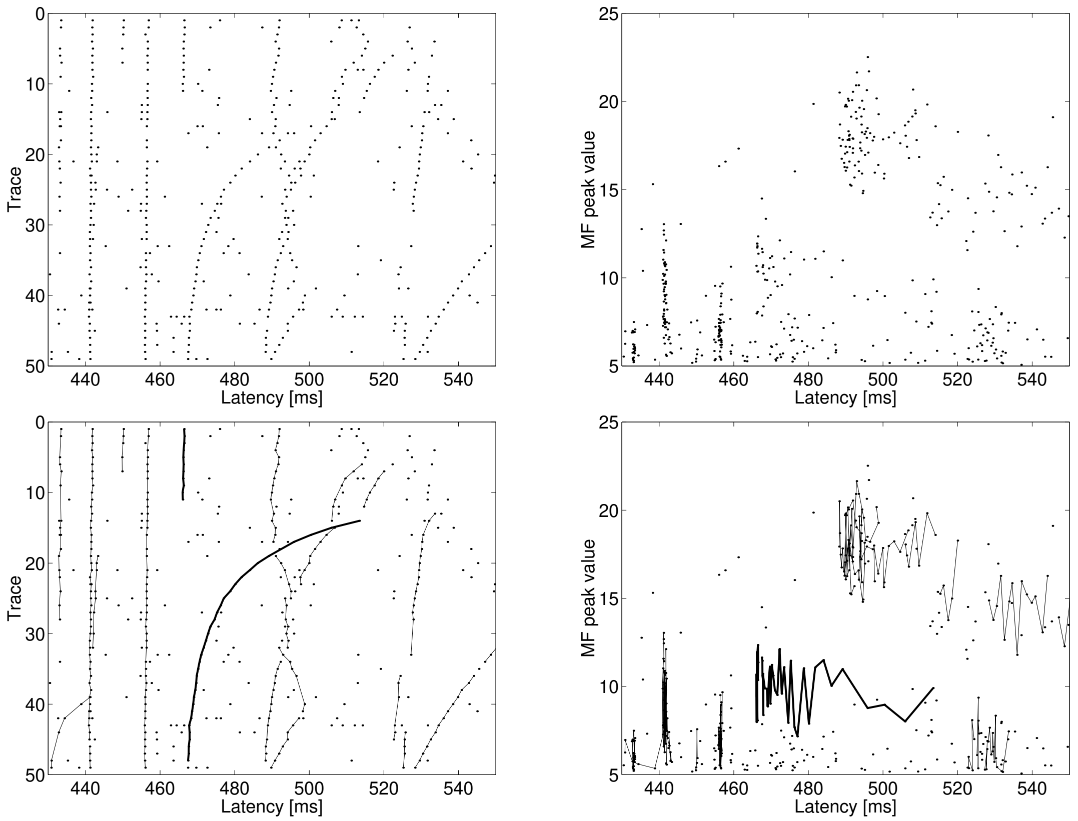

Fig. 11. A result of the current algorithm where several units were recorded with crossing trajectories. Both the time course (top left) and the amplitude information (top right) of the detected APs are shown. The tracking result is included and the activated unit is marked with a thick line (bottom left and bottom right). The method handles crossing tracks well because the amplitude of the APs differ.

presented. The objective of the application was to quantitatively estimate conduction latency shifts and post-stimulus recovery constants of human nerve C-fibers.

The APs were successfully detected by means of a matched filter constituting an optimal ML-CFAR detector. Even APs with amplitudes of the same order of magnitude as the peaks of the noise were detected correctly.

The discrimination between APs originating from different C-fibers was carried out using the MHT method as described in [13]. Only some minor changes were introduced to adapt the method to the application described. The results corresponded well with what an experienced physician would consider to be a "correct" result.

One set of the two desired parameters, latency shift and recovery constant, were estimated from a tracked recovery using an exponential decay model. A good fit was found through a combination of the simplex method and the least squares method. Using non-linear statistics, confidence intervals were derived and presented. The residuals were small and the exponential curve corresponded well with the recovery.

In spite of the good performance, some minor aspects could still be improved. In the matched filter derivation, for example, the noise was assumed to be white. As this is not the case, the color of the noise should have been considered when the MF impulse response was tuned. Despite this deficiency, the matched filter detector has shown to perform well for non-white noise recordings as well as to be robust to a wide range of AP shapes.

The most obvious drawback of the MHT algorithm is its exhaustive computational and storage requirements. In the cases considered so far, these requirements have, however, not been a limiting factor. If they were, the track oriented MHT implementation could be used as its computational and storage requirements are less exhaustive [29] [30].

The reason for choosing the MHT method in spite of its complexity is that it is considered to be one of the best tracking methods regarding to performance. Other methods have various shortcomings, for example, the low track maintenance of the nearest neighbor (NN) association method, and the typical track switching behavior of the joint probabilistic data association (JPDA) method are not acceptable [16].

Another drawback of the current implementation is its sensitivity to errors in the model parameter α that represents an a priori value of the recovery time constant of the latency. It is reasonable to believe, however, that introducing robust filtering methods [31] [32] or replacing the Kalman predictor with an MM-based predictor, the filtering could be made less sensitive to differences in the recovery constant. Implementing the MM approach would probably be the most straight-forward, because the number of observations to initiate the predictor could be kept low. Otherwise, some iterative initiation procedure would probably have to be included.

The parameter estimation residuals, finally, were neither Gaussian nor white due to model errors in the model. Also, the estimated confidence intervals of the parameters estimated were larger than the true confidence intervals (not shown in the paper). To improve on the model errors in the parameter estimation, one could fit an exponential function with two exponential terms. By doing so, an improved result in terms of the model errors is obtained. However, the already oversized confidence intervals become even larger; too large to be useful. These deficiencies exist because the parameter estimation is based on a theory that is only asymptotically correct and because the trajectory lengths considered in this type of application are too short in this regard.

To further improve the performance of the algorithm, future work should include a noise covariance matrix estimator and an MM-based target predictor. If possible, a better model of the latency recovery together with a more appropriate statistical analysis of the parameter estimation would be valuable.

To sum up, the goal of simplifying and improving the efficiency of the analysis of the human nerve C-fiber recordings has been reached. The computer application developed based on this paper has already shown to be useful to the research team. In the practical cases considered so far, the overall performance of the application has been promising.

IX. Acknowledgements

Financial support was obtained from the Swedish Medical Research Council, Proj. no. 5206, the Deutsche Forschungsgemeinschaft (SFB 353), and a Max Planck Research Award to Erik Torebjörk.

The authors would like to thank Prof. Anders Ahlén and Prof. Mikael Sternad for valuable comments regarding this work.

TABLE II
MHT PARAMETERS

Description	*Parameter*		*Value*
A priori det. prob.	$\bar{P}_D(k_0)$		0.6
Min det. prob.	$\bar{P}_{D,min}$		0.5
Max det. prob.	$\bar{P}_{D,max}$		0.9999
Forgetting factor	λ_{P_D}		0.1
New target intensity	β_{NT}	[ms^{-1}]	10^{-7}
False target intensity	β_{FT}	[ms^{-1}]	$2.5 \cdot 10^{-5}$
Gate size	G		12
Deletion score	L_{del}		0
Deletion miss count	N_{del}		3
Confirmation score	L_{conf}		6
Root node depth	N_{prune}		3
Max # hypotheses	N_{max}		16
Lat. process variance	$\sigma^2_{e_1}$	[ms^{-1}]	$2 \cdot 10^{-5}$
Ampl. process variance	$\sigma^2_{e_2}$	[ms^{-1}]	10^{-7}
Process noise constant	β_0		3
Process noise decay	β_1		0.05
Lat. meas. variance	$q^{(2)}_{11}$	[ms^2]	0.05
Ampl. meas. variance	$q^{(2)}_{11}$		1
Max lat. derivative	$\dot{y}^{(1)}_{max}$		3
Recovery constant	α	[ms^{-1}]	0.0375
Stimulation period	T	[ms]	4

Appendix

A. The matched filter for colored noise

In cases where the color of the noise may not be neglected, the optimal impulse response and the output SNR of the matched filter should be replaced by

$$\mathbf{h}_o = \frac{\mathbf{R}^{-1}_{\boldsymbol{\eta\eta}}\mathbf{s}}{\sqrt{\mathbf{s}^T\mathbf{R}^{-1}_{\boldsymbol{\eta\eta}}\mathbf{s}}}; \quad SNR_{mf} = \gamma^2\mathbf{s}^T\mathbf{R}^{-1}_{\boldsymbol{\eta\eta}}\mathbf{s} \tag{66}$$

where $\mathbf{R}_{\boldsymbol{\eta\eta}}$ is the $p|p$ covariance matrix of the noise $\boldsymbol{\eta}(t)$, see (5).

B. MHT parameter and algorithm specifics

For the interested reader, the MHT parameter settings used in this paper are listed in Table II.

Since the detection probability P_D may change during the experiment, it is estimated using the recursion

$$\bar{P}_D(k) \triangleq (1-\lambda_{P_D})\bar{P}_D(k-1) + \lambda_{P_D}\hat{P}_D(k) \tag{67}$$

$$\hat{P}_D(k) \triangleq 1 - \Phi(m_0 - \mathbf{c}_2^T\hat{\mathbf{x}}(k|k)), \quad k > k_0 \tag{68}$$

where λ_{P_D} is a forgetting factor and $\mathbf{c}_2^T$ is the second row in the measurement matrix $\mathbf{H}$. This estimate has, however, a positive bias for small APs as the MF output values below the threshold do not contribute. The bias may be calculated and the estimate corrected, but it is believed to be of small importance (to the tracking result) and is therefore not considered.

The actual detection probability, from the tracker's perspective, is the mutual probability of the MF detection and the gating. Normally, only large gates are interesting and the effect of the gating is consequently neglected.

Following [29], the *track score* may be calculated recursively as

$$L_i(k) = L_i(k-1) + \Delta L_i(k), \quad k > k_0+1 \tag{69}$$

$$\Delta L_i(k) \triangleq \begin{cases} \ln(1-P_D), & \text{not updated} \\ \ln\left[\frac{P_D}{\beta_{FT}2\pi\sqrt{|\mathbf{S}_{il}|}}\right] - d^2_{il}, & \text{updated} \end{cases} \tag{70}$$

$$L_i(k_0) \triangleq \ln\left[1 + \frac{\beta_{NT}}{\beta_{FT}}\right] \tag{71}$$

$$L_i(k_0+1) \triangleq \ln\frac{\beta_{NT}}{\beta_{FT}} + \ln\left[\frac{P_D}{\beta_{FT}2\pi\sqrt{|\mathbf{S}_{i1}|}}\right] - \ln d^2_{i1} \tag{72}$$

where β_{FT} and β_{NT} are the false alarm and the new source density, respectively, and d^2_{il} is the normalized distance for the lth observation of track i. As the tracking filter needs one update (two observations) to initialize, all potential tracks with a missed detection are rejected. This results in a simplified score calculation of tentative tracks as given (72). Also, experience has shown that better performance is achieved when $\ln d^2_{i1}$ is used instead of only d^2_{i1}. This gives a slight preference to tracks with a stable latency.

Using the track score, the hypothesis score at scan k may be written

$$L(k) = \sum_{i=1}^{n_k} L_i(k) + \tilde{L} \tag{73}$$

where $L_i(k)$ is the track score, $\tilde{L}$ is the *residual hypothesis score* due to track termination, and n_k is the number of targets (tracks) associated with this hypothesis at scan k.

C. Derivation of the discrete time process noise covariance matrix

The covariance matrix $\mathbf{Q}_1(k)$ of the sampled process noise is defined by (29) and (30). As $\mathbf{dw}(\nu)$ and $\mathbf{dw}(\tau)$ are independent for $\nu \neq \tau$, we obtain the expression (76) where the matrix elements q_{ij}, and ρ_{ij} are given by (77)-(79), and (80)-(83), respectively. The diagonal covariance matrix $\Lambda(kT)$ is given by (25), and the diagonal matrices $\Sigma(kT)$, and Σ_0 are given by

$$\Sigma(kT) = \begin{pmatrix} 1 & 0 & 0 \\ 0 & 1 & 0 \\ 0 & 0 & 0 \end{pmatrix} \sigma_{e_1}^2 e^{\beta_0 - \beta_1 (k-k_0)T} \tag{84}$$

$$\Sigma_0 = \begin{pmatrix} \sigma_{e_1}^2 & 0 & 0 \\ 0 & \sigma_{e_1}^2 & 0 \\ 0 & 0 & \sigma_{e_2}^2 \end{pmatrix}. \tag{85}$$

D. Derivation of the LS-estimates of the initial state vector and its covariance matrix

By direct iteration of the model (26)-(33) and assuming a correct model, i.e. no process noise, the LS-estimate of the initial state vector $\hat{\mathbf{x}}(k_0+2|k_0+1)$ and its covariance matrix $\mathbf{P}(k_0+2|k_0+1)$ is

$$\hat{\mathbf{x}}(k_0+2|k_0+1) = \mathcal{U} \begin{pmatrix} \mathbf{y}(k_0) \\ \mathbf{y}(k_0+1) \end{pmatrix} \tag{86}$$

$$\mathbf{P}(k_0+2|k_0+1) = \mathcal{U} \begin{pmatrix} \mathbf{Q}_2 & \mathbf{0}_{22} \\ \mathbf{0}_{22} & \mathbf{Q}_2 \end{pmatrix} \mathcal{U}^T + \mathbf{Q}_1(k_0+1) \tag{87}$$

$$\mathcal{U} \triangleq \mathbf{F}^2 (\mathcal{O}_1^T \mathcal{O}_1)^{-1} \mathcal{O}_1^T \tag{88}$$

where $\mathbf{0}_{ij}$ is a $i|j$ dimensional zero matrix and $\mathcal{O}_1$ is the $4|3$ partial observability matrix defined as [33]

$$\mathcal{O}_1 \triangleq \begin{pmatrix} \mathbf{H} \\ \mathbf{HF} \end{pmatrix}. \tag{89}$$

If one accounts for the process noise, the following matrix $\mathbf{Q}_0$ should (formally) be added to $\mathbf{P}(k_0+2|k_0+1)$

$$\mathcal{U}_0 \triangleq \mathbf{F}(\mathcal{O}_1^T \mathcal{O}_1)^{-1} \mathcal{O}_1^T \begin{pmatrix} \mathbf{0}_{23} \\ \mathbf{H} \end{pmatrix} \tag{90}$$

$$\mathbf{Q}_0 \triangleq (I - \mathcal{U}_0) \mathbf{Q}_1(k_0+1)(I - \mathcal{U}_0)^T. \tag{91}$$

The intermediate state vector $\hat{\mathbf{x}}(k_0+1|k_0)$ and its "covariance" matrix $\mathbf{P}(k_0+1|k_0)$ are needed for the gating of the first candidate update, but they may not be properly calculated. Nevertheless, practical values, although ad hoc, may be calculated through

$$\hat{\mathbf{x}}(k_0+1|k_0) = \begin{pmatrix} 1 & 0 \\ 0 & 0 \\ 0 & 1 \end{pmatrix} \mathbf{y}(k_0) \tag{92}$$

$$\mathbf{P}(k_0+1|k_0) = \begin{pmatrix} \mathbf{P}_{11} & \mathbf{0}_{21} \\ \mathbf{0}_{12} & \mathbf{P}_{22} \end{pmatrix} \tag{93}$$

$$\mathbf{P}_{11} \triangleq \begin{pmatrix} 1 & 0 \\ 0 & 0 \end{pmatrix} \frac{(\dot{y}_{max}^{(1)} T)^2}{G} \tag{94}$$

$$\mathbf{P}_{22} \triangleq 2 q_{22}^{(2)} \tag{95}$$

where $\dot{y}_{max}^{(1)}$ is the maximum latency derivative that should be allowed in the gating condition and G is the gate size.

Björn Hammarberg (Hansson) was born in Östersund, County of Jämtland, Sweden, in 1970. He received the M.Sc. degree in engineering physics from Uppsala University in 1995. Since then, he has been working at the Department of Clinical Neurophysiology at University Hospital, Uppsala, with signal processing in various medical applications. For a shorter period during the fall of 1995, he was at the Department of Clinical Neurophysiology, Institute of Neurology, at Nijmegen University Hospital, working on an EMG decomposition system to the needs of the department. Since the spring of 1996, he has been working towards a Ph.D. degree in signal processing of neurophysiological data at the Signals and Systems Group at Uppsala University.

Clemens Forster received the M.S. degree in computational science for medicine, in 1984, and the Ph.D. degree for biomedical science, in 1991, from the University of Heidelberg, Germany. He worked for several years as a research assistant in the development of systems for recording and analysis of neurophysiological data. He is currently at the Department of Physiology and Experimental Pathophysiology at the University of Erlangen-Nuernberg where he is a member of the pain research group. His main research interests are in the fields of biomedical signal processing and analysis of pain related brain areas using functional magnetic resonance imaging.

Erik Torebjörk . . . .

References

[1] H. E. Torebjörk and R. G. Hallin, "C-fibre units recorded from human sensory nerve fascicles in situ," *Acta Soc. Med. Ups.*, vol. 75, pp. 81–84, 1970.

[2] R. G. Hallin and H. E. Torebjörk, "Afferent and efferent C units recorded from human skin nerves in situ," *Acta Soc. Med. Ups.*, vol. 75, pp. 277–281, 1970.

$$\mathbf{Q}_1(k) \stackrel{\triangle}{=} E\int_0^T e^{\mathbf{A}(T-\tau)}\mathbf{G}\,\mathbf{dw}(kT+\tau)\mathbf{dw}^T(kT+\tau)\,\mathbf{G}^T e^{\mathbf{A}^T(T-\tau)} \tag{74}$$

$$= \int_0^T e^{\mathbf{A}(T-\tau)}\mathbf{G}\Lambda(kT+\tau)\mathbf{G}^T e^{\mathbf{A}^T(T-\tau)}\,d\tau \tag{75}$$

$$= \begin{pmatrix} q_{11} & q_{12} & 0 \\ q_{21} & q_{22} & 0 \\ 0 & 0 & 0 \end{pmatrix}\Sigma(kT) + \begin{pmatrix} \rho_{11} & \rho_{12} & 0 \\ \rho_{21} & \rho_{22} & 0 \\ 0 & 0 & \rho_{33} \end{pmatrix}\Sigma_0 \tag{76}$$

$$q_{11} = \alpha^{-2}\left(\beta_1^{-1}(1-e^{-\beta_1 T}) - 2(\beta_1-\alpha)^{-1}(e^{-\alpha T}-e^{-\beta_1 T}) + (\beta_1-2\alpha)^{-1}(e^{-2\alpha T}-e^{-\beta_1 T})\right) \tag{77}$$

$$q_{12} = q_{21} = \alpha^{-1}\left((\beta_1-\alpha)^{-1}(e^{-\alpha T}-e^{-\beta_1 T}) - (\beta_1-2\alpha)^{-1}(e^{-2\alpha T}-e^{-\beta_1 T})\right) \tag{78}$$

$$q_{22} = (\beta_1-2\alpha)^{-1}(e^{-2\alpha T}-e^{-\beta_1 T}) \tag{79}$$

$$\rho_{11} = \alpha^{-2}\left(T-(2\alpha)^{-1}(3-4e^{-\alpha T}+e^{-2\alpha T})\right) \tag{80}$$

$$\rho_{12} = \rho_{21} = \alpha^{-1}(2\alpha)^{-1}\left(1-e^{-\alpha T}\right)^2 \tag{81}$$

$$\rho_{22} = (2\alpha)^{-1}(1-e^{-2\alpha T}) \tag{82}$$

$$\rho_{33} = T \tag{83}$$

[3] C. Forster and M. Schmelz, "New developments in microneurography of human C fibers," *News in Physiological Sciences*, vol. 11, pp. 170–175, 1996.

[4] H. E. Torebjörk and R. G. Hallin, "Responses in human A and C fibres to repeated electrical intradermal stimulation," *J. Neurol. Neurosurg. Psychiatry*, vol. 37, pp. 653–664, 1974.

[5] M. Schmelz, R. Schmidt, M. Ringkamp, C. Forster, H. O. Handwerker, and H. E. Torebjörk, "Limitation of sensitization to injured parts of receptive fields in human skin C-nociceptors," *Exp. Brain Res.*, vol. 109, pp. 141–147, 1996.

[6] M. Schmelz, C. Forster, R. Schmidt, M. Ringkamp, H. O. Handwerker, and H. E. Torebjörk, "Delayed responses to electrical stimuli reflect C-fiber responsiveness in human microneurography," *Exp. Brain Res.*, vol. 104, pp. 331–336, 1995.

[7] C. Forster and H. O. Handwerker, "Automatic classification and analysis of microneurographic spike data using a PC/AT," *J. Neurosci. Methods*, vol. 31, pp. 109–118, 1990.

[8] R. Schmidt, M. Schmelz, C. Forster, M. Ringkamp, H. E. Torebjörk, and H. O. Handwerker, "Novel classes of responsive and unresponsive C nociceptors in human skin," *J. Neurosci.*, vol. 15, pp. 333–341, 1995.

[9] C. Weidner, M. Schmelz, B. Hansson, H. O. Handwerker, and H. E. Torebjörk, "Functional attributes discriminating mechano-insensitive and mechano-responsive C nociceptors in human skin," *J. Neurosci.*, vol. 19, pp. 10184–10190, Nov. 1999.

[10] K. Lundin, "A system for analysis of human pain signals using a radar tracking approach," M.S. thesis, UPTEC F 98 078, Uppsala University, Uppsala, Sweden, Oct. 1998.

[11] B. Hansson, C. Forster, and E. Torebjörk, "Matched filtering and multiple hypothesis tracking applied to C-fiber action potentials recorded in human nerves," in *Proc. of SPIE, Signal and Data Processing of Small Targets*, Orlando, FL, Sept. 1998, vol. 3373, pp. 582–593.

[12] J. A. Cadzow, "Matched filters," in *Foundations of Digital Signal Processing and Data Analysis*, pp. 442–461. Macmillan, New York, NY, 1987.

[13] S. S. Blackman, *Multiple-Target Tracking with Radar Applications*, Artech House, Dedham, MA, 1986.

[14] A. Steinhardt, "Adaptive multisensor detection and estimation," in *Adaptive Radar Detection and Estimation*, pp. 91–160. Wiley, New York, NY, 1992.

[15] D. B. Reid, "An algorithm for tracking multiple targets," *IEEE Trans. on Automatic Control*, vol. 24, no. 6, pp. 843–854, Dec. 1979.

[16] M. de Feo, A. Graziano, R. Miglioli, and A. Farina, "IMMJPDA versus MHT and Kalman filter with NN correlation: performance comparison," *IEE Proc.-Radar, Sonar Navig.*, vol. 144, no. 2, pp. 49–56, 1997.

[17] Y. Bar-Shalom, "Extension of the probabilistic data association filter in multi-target tracking," in *Proc. 5th Symp. on Nonlinear Estimation*, Sept. 1974, pp. 16–21.

[18] S. Haykin, *Adaptive Filter Theory*, Prentice Hall, Englewood Cliffs, NJ, second edition, 1991.

[19] D. Lerro and Y. Bar-Shalom, "Interacting multiple model tracking with target amplitude feature," *IEEE Trans. on Aerospace and Electronic Systems*, vol. 29, no. 2, pp. 494–508, 1993.

[20] Y. Bar-Shalom and X.-R. Li, *Estimation and Tracking: Principles, Techniques, and Software*, Artech House, Norwood, MA, 1993.

[21] D. T. Magill, "Optimal adaptive estimation of sampled stochastic processes," *IEEE Trans. on Automatic Control*, vol. 10, pp. 434–439, 1965.

[22] K. J. Åström, "Stochastic state models," in *Introduction to Stochastic Control Theory*, pp. 44–90. Academic Press, New York, NY, 1970.

[23] K. J. Åström and B. Wittenmark, "Discrete-time systems," in *Computer Controlled Systems, Theory and Design*, pp. 30–76. Prentice Hall, Upper Saddle River, NJ, 1997.

[24] J. E. Dennis, Jr. and D. J. Woods, *New Computing Environments: Microcomputers in Large-Scale Computing*, pp. 116–122, SIAM, 1987.

[25] J. C. Lagarias, J. A. Reeds, M. H. Wright, and P. E. Wright, "Convergence properties of the Nelder-Mead simplex method in low dimensions," *SIAM Journal on Optimization*, vol. 9, no. 1, pp. 112–147, 1998.

[26] L. Råde and B. Westergren, *BETA: Mathematics Handbook*, Studentlitteratur, Lund, Sweden, 1989.

[27] R. A. Gallant, "Univariate nonlinear regression," in *Nonlinear Statistical Models*, chapter 1, pp. 1–122. Wiley, New York, NY, 1987.

[28] H. E. Torebjörk, "Afferent C units responding to mechanical, thermal and chemical stimuli in human non-glabrous skin," *Acta physiol. scand.*, vol. 92, pp. 374–390, 1974.

[29] S. S. Blackman, R. J. Dempster, and S. H. Roszkowski, "IMM/MHT applications to radar and IR multitarget tracking," in *Proc. of SPIE, Signal and Data Processing of Small Targets 1997*, Orlando, FL, Oct. 1997, vol. 3163, pp. 429–439.

[30] J. R. Werthman, "Step-by-step description of a computationally efficient version of multiple hypothesis tracking," in *Proc. of SPIE, Signal and Data Processing of Small Targets 1992*, Aug. 1992, vol. 1698, pp. 288–300.

[31] M. Sternad, K. Öhrn, and A. Ahlén, "Robust $\mathcal{H}_2$ filtering for structured uncertainty: the performance of probabilistic and minimax schemes," in *Proc. of 3rd European Control Conf.*, Rome, Italy, 1995, vol. 1, pp. 87–92.

[32] K. Öhrn, *Design of Multivariable Cautious Discrete-Time Wiener Filters: A Probabilistic Approach*, Ph.D. thesis, Uppsala University, Uppsala, Sweden, 1996.

[33] T. Kailath, *Linear Systems*, Prentice Hall, Englewood Cliffs, NJ, 1980.